Silicon-on-Insulator Passive Photonics Structures

YOUNUS MANDALAWI

[1]*TU Braunschweig, Braunschweig, 38106, Germany*
**y.mandalawi@tu-braunschweig.de*

Abstract: Silicon photonics integrated circuits have been implemented in many systems, from communications to sensing. In this report, a 500 nm width and 220 nm thick silicon-on-insulator strip waveguide is designed with Ansys Lumerical for around 1550 nm wavelength. The waveguide is then utilized to design a layout with SiEPIC PDK and KLayout. This includes different MZI and ring resonators. After the layout's tapout and manufacturing, the experimental results are compared with simulations.

1. Introduction

Silicon photonics integrated circuits offer many advantages such as low-power consumption, high bandwidth, immunity to electromagnetic interference, and compatibility with standard CMOS manufacturing [1–6]. Therefore, it has been implemented in a wide variety of systems for performance improvement or for overcoming the limitations of pure electronic systems. Silicon photonics integrated circuits have been utilized in many applications such as optical and THz communications, optical sensing, and space applications.

Here, the main objective of this report is to design a silicon photonics waveguide for around 1550 nm wavelength. The design and tested silicon waveguide is a 500 nm width and 220 nm height strip waveguide. Only the main TE mode is used. Different MZI and ring resonator structures are constructed with Ansys Lumerical, SiEPIC PDK, and KLayout software. The frequency response of such structures is shown. Additionally, the experimental results are also reported as a validation of such designs.

2. Main Waveguide

The silicon waveguide with 500 nm width and 220 nm height is depicted in Fig. 1. The waveguide supports TE and TM modes at around 1550 nm wavelength. The simulation of the waveguide was done with a finite difference eigenmode solver from Ansys Lumerical [6].

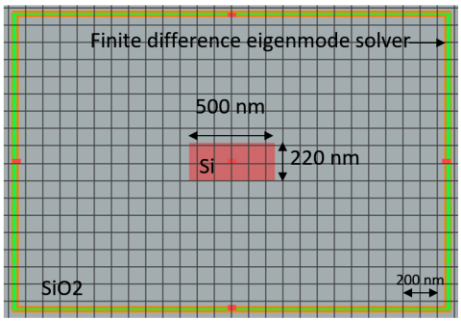

Fig. 1. Waveguide structure XZ view.

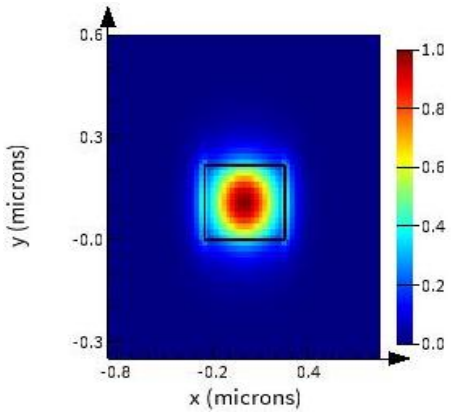

Fig. 2. TE mode.

Figure 2 shows the TE mode intensity at 1550 nm, which indicates a clear confinement inside the waveguide geometry where the mode is fully guided.

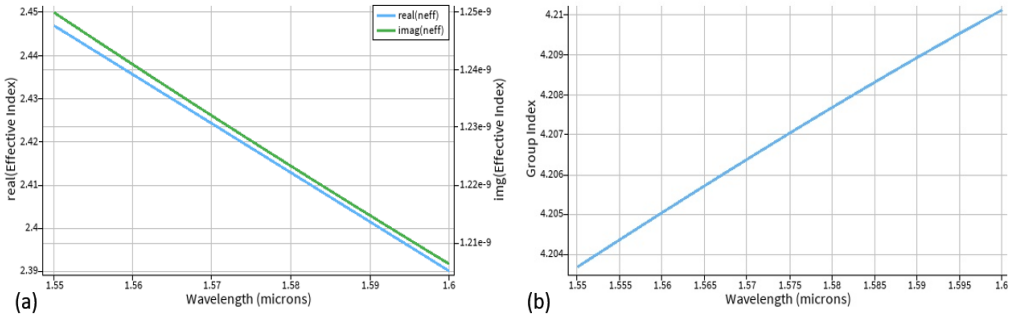

Fig. 3. (a) Effective index vs wavelength. (b) Group index vs wavelength.

In Fig. 3(a), the effective index is plotted against the from 1550 nm to 1600 nm, which decreases with the wavelength. The effective index at 1550 nm is 2.45. The resulting group index as a function of wavelength is exhibited in Fig. 3(b) with 4.20 group index at 1550 nm wavelength. By doing a second-order polynomial fitting of the effective index n_{eff} with wavelength λ curve, the polynomial coefficients n_1, n_2, and n_3 are extracted. Then, a Taylor expansion around the center wavelength λ_0 is implemented as follows to create a compact waveguide model [6]:

$$n_{\text{eff}}(\lambda) = n_1 + n_2(\lambda - \lambda_0) + n_3(\lambda - \lambda_0)^2 \quad (1)$$

For our waveguide, n_1, n_2, and n_3 are 2.44366, 1.13315, and -0.0400796, respectively. At λ_0 , the n_{eff} equal to n_1, while the group index n_{g} is $n_1 - n_2\lambda_0$.

3. Simulation Structure Design and Results

Different structures are designed and simulated with Ansys Lumerical, SiEPIC PDK and KLayout software.

3.1 MZI

One important structure is the Mach-Zehnder interferometer or MZI. It is used as the basic building block in many photonics systems. This includes but is not limited to filters and switches. In the simplest scenario, it consists of two Y-branches connecting two arms of the MZI. The FSR of an MZI has an inverse relation with the length difference between the two arms ΔL. This can be calculated as [6]:

$$FSR = (\lambda)^2/(n_g \cdot \Delta L) \quad (2)$$

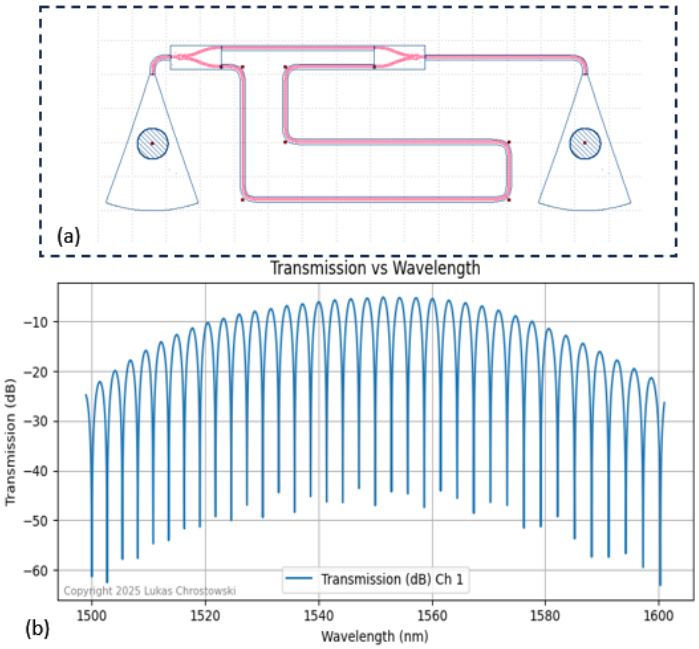

Fig. 4. (a) MZI1 and MZI2 with $\Delta L = 200\ \mu m$. The aim is to show the manufacturing variation effect on FSR. (b) MZI1 and MZI2 transmission versus wavelength with 2.86 nm *FSR*.

Figure 4(a) shows the design for an MZI with $\Delta L = 200\ \mu m$. The MZI transmission as a function of wavelength from 1500 nm to 1600 nm is depicted in Fig. 4(b). The calculated FSR is around 2.86 nm. For shorter FSR, the length difference should be increased. Fig. 5(a) shows the design for an MZI with $\Delta L = 344\ \mu m$. The MZI transmission as a function of wavelength from 1500 nm to 1600 nm is depicted in Fig. 5(b). The calculated FSR is around 1.66 nm.

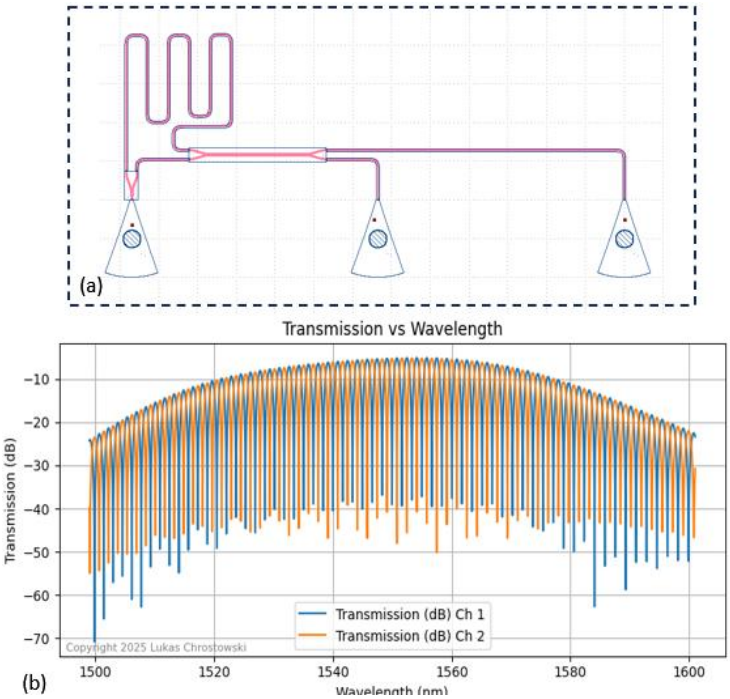

Fig. 5. MZI3 has two output ports to show constructive and destructive interferences. The $\Delta L = 344\ \mu m$. (b) Transmission versus wavelength for MZI3 with 1.66 nm FSR.

Much longer $\Delta L = 1200\ \mu m$ is also designed. Fig. 6(a) shows the design for an MZI with $\Delta L = 1200\ \mu m$. The MZI transmission as a function of wavelength from 1500 nm to 1600 nm is depicted in Fig. 5(b). The calculated FSR is around 0.476 nm.

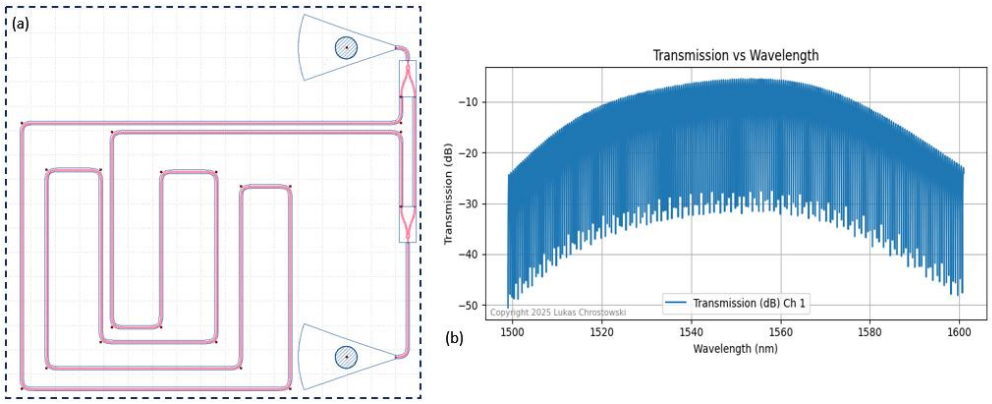

Fig. 6. (a) MZI4 and MZI5 both have much longer $\Delta L = 1200\ \mu m$ to show the shorter FSR and compare both for fabrication tolerance. (b) Transmission versus wavelength for MZI5 and MZI6 with 0.476 nm FSR.

MZI structures with different ΔL can be cascaded to create a pattern in the response, hence they are used as a filter, for example. Fig. 7(a) presents a design with 4 cascaded MZIs with $\Delta L1 = 50\ \mu m$, $\Delta L2 = 60\ \mu m$, $\Delta L3 = 55\ \mu m$, $\Delta L4 = 65\ \mu m$ from top to bottom. The transmission response is plotted in Fig. 7(b).

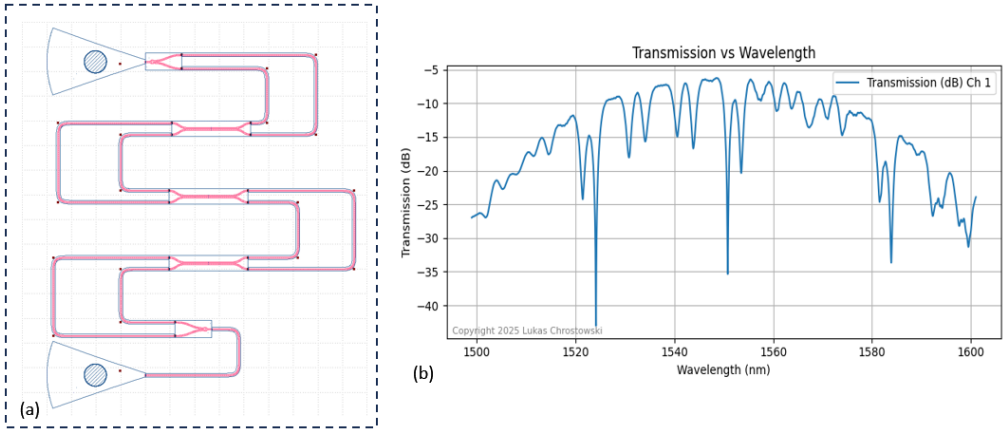

Fig. 7. (a) MZI6 has four cascaded MZIs with $\Delta L1 = 50\ \mu m$, $\Delta L2 = 60\ \mu m$, $\Delta L3 = 55\ \mu m$, $\Delta L4 = 65\ \mu m$. The idea is to create a pattern. Similar structures are used to create a wideband optical bandpass filter, for example. (b) Transmission versus wavelength for MZI4.

3.2 Ring Resonator

Another well-known structure is the ring resonator. It consists of single or double bus waveguides and a coupled ring with R radius. In this case, the FSR can be calculated as:

$$FSR = (\lambda)^2/(n_g \cdot 2 \cdot \pi \cdot R) \qquad (3)$$

Figure 8(a) exhibits a double-bus ring resonator with a 10 μ radius and a gap of 100 nm between the bus and the ring.

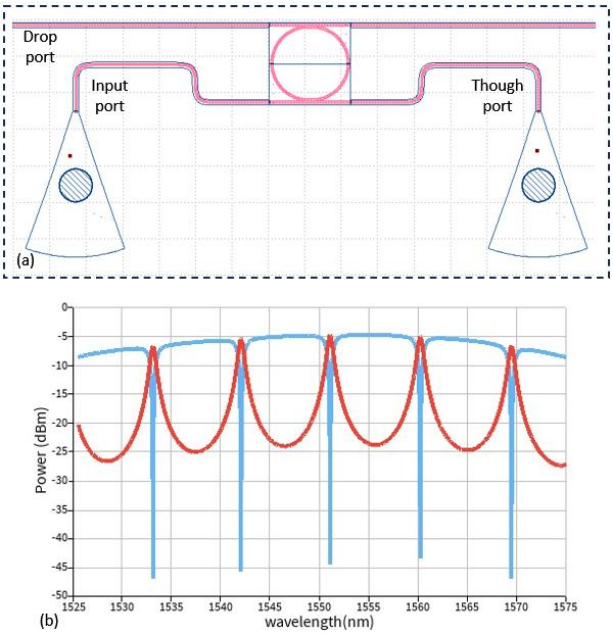

Fig. 8 (a) Double-bus ring resonator (RING1) with 10 μm radius. (b) RING1 transmission versus wavelength for drop-port (red), though-port (blue), with around 9.10 nm FSR.

Figure 8(b) displays the response of the ring resonator for the through-port (blue) and also the drop-port (red). The calculated FSR is around 9.10 nm.

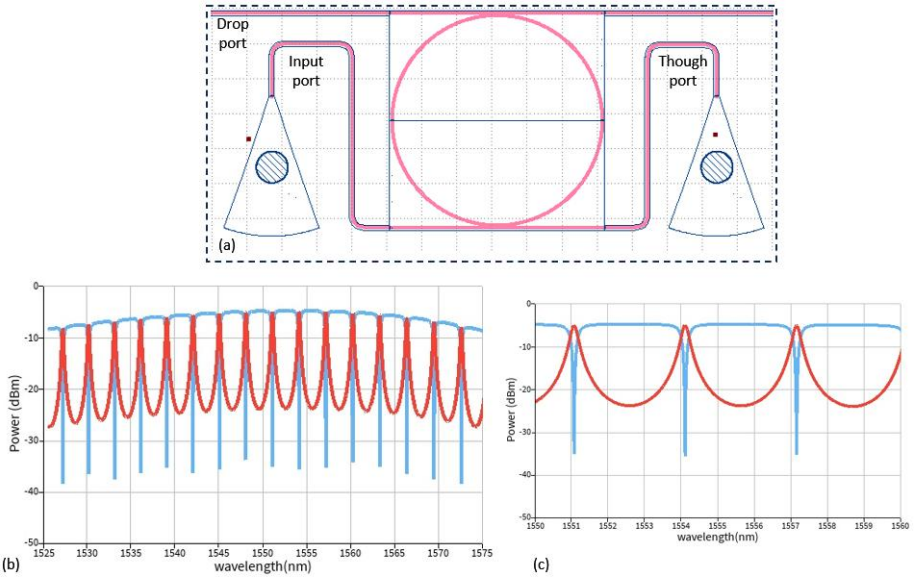

Fig. 9 (a) Double-bus ring resonator (RING1) with 30 μm radius. (b) RING1 transmission versus wavelength for drop-port (red), though-port (blue), with around 3.03 nm FSR. (c) Zoomed version from 1550 nm to 1560 nm.

Figure 9(a) exhibits a double-bus ring resonator with a larger 30 μ radius and a gap of 100 nm between the bus and the ring. Figure 8(b) displays the response of the ring resonator for the through-port (blue) and also the drop-port (red). The calculated FSR is around 3.03 nm.

4. Experimental Results

4.1 MZI

Use an initial capital for the first word in the title and for proper nouns. Use lowercase following a colon. The title should not begin with “A,”, “An,” or “The” or contain the words "first," "new," or "novel."

3.2 Ring Resonator

Author names should be styled as follows: first and middle names (given names) or initials followed by surname. Please keep author names consistent from one paper to the next within our publications.

3.3 Author affiliations

Only one single corresponding author may be identified for a manuscript. The corresponding author typically is the person who submits the manuscript and handles correspondence throughout the peer review and publication process. Alternatively, you may choose not to identify a corresponding author and instead use an author note to indicate equal author contributions. Only the corresponding author will have an asterisk attached to their email address. Additional co-author e-mail addresses will have a superscript number in the numerical order of the affiliations.
shapes for data points, text labels pointing to the color features, numbering, etc.

Tables should be centered and numbered consecutively in the order they are cited in the paper. Authors must use Word's Table editor to insert tables. **Do not import tables from Excel.** All content for each table should be in a single Word table (do not split content for a single table across multiple Word tables). Use horizontal lines to delimit the top and bottom of the table

References

1. W. N. Ye and Y. Xiong, "Review of silicon photonics: History and recent advances," J. Mod. Opt. **60**(16), 1299–1320 (2013).

2. L. R. Chen, "Integrated Microwave Photonics," 2021 International Topical Meeting on Microwave Photonics, MWP 2021 1–4 (2021).

3. Y. Shi, Y. Zhang, Y. Wan, Y. Yu, Y. Zhang, X. Hu, X. Xiao, H. Xu, L. Zhang, and B. Pan, "Silicon photonics for high-capacity data communications," Photonics Res. **10**(9), A106 (2022).

4. S. Y. Siew, B. Li, F. Gao, H. Y. Zheng, W. Zhang, P. Guo, S. W. Xie, A. Song, B. Dong, L. W. Luo, C. Li, X. Luo, and G. Q. Lo, "Review of Silicon Photonics Technology and Platform Development," Journal of Lightwave Technology **39**(13), 4374–4389 (2021).

5. S. Shekhar, W. Bogaerts, L. Chrostowski, J. E. Bowers, M. Hochberg, R. Soref, and B. J. Shastri, "Roadmapping the next generation of silicon photonics," Nat. Commun. **15**(1), (2024).

6. L. Chrostowski and M. Hochberg, *Silicon Photonics Design* (Cambridge University Press, 2015).